PHYSICAL REVIEW B **94**, 094411 (2016)

Magnetic structures of the Eu and Cr moments in $EuCr_2As_2$: Neutron diffraction study

S. Nandi,[1,*] Y. Xiao,[2,†] N. Qureshi,[3] U. B. Paramanik,[1] W. T. Jin,[2,4] Y. Su,[4] B. Ouladdiaf,[3] Z. Hossain,[1] and Th. Brückel[2,4]

[1]*Department of Physics, Indian Institute of Technology, Kanpur 208016, India*

[2]*Jülich Centre for Neutron Science JCNS and Peter Grünberg Institut PGI, JARA-FIT, Forschungszentrum Jülich GmbH, D-52425 Jülich, Germany*

[3]*Institut Laue Langevin, 71 rue des Martyrs, BP156, 38042 Grenoble Cedex 9, France*

[4]*Jülich Centre for Neutron Science JCNS, Forschungszentrum Jülich GmbH, Outstation at MLZ, Lichtenbergstraße 1, D-85747 Garching, Germany*

(Received 21 June 2016; revised manuscript received 9 August 2016; published 12 September 2016)

The magnetic structures of the Eu^{2+} and Cr^{2+} moments in the nonsuperconducting parent compound $EuCr_2As_2$ have been determined by using neutron diffraction. While the Eu^{2+} moments order ferromagnetically with moments along the **c** direction at $T_C = 21.0(1)$ K, the ordering temperature of the Cr^{2+} moments is found to be at very high temperature of 680(40) K by using magnetization measurements. The Cr^{2+} moments order in a *G*-type antiferromagnetic structure with moments along the **c** direction. According to this magnetic structure, the nearest-neighbor Cr^{2+} moments are antiferromagnetically aligned in the *a*-*b* plane as well as in the **c** direction. The ordered magnetic moment of the Eu^{2+} and Cr^{2+} amounts to $6.2(5)\mu_B$ and $1.7(4)\mu_B$, respectively, at $T = 2$ K.

DOI: 10.1103/PhysRevB.94.094411

I. INTRODUCTION

The discovery of iron-based superconductors [1] in 2008 has attracted worldwide attention in the unconventional high-T_{SC} (T_{SC} is the superconducting transition temperature) superconductivity research [2]. Among various classes of Fe-based superconductors [1,3–7], the ternary "122" system, AFe_2As_2 (A = Ba, Ca, Sr, Eu, K, Rb, and Cs) with T_{SC} up to 38 K [8–11], has been the most widely studied member of Fe-pnictide superconductors. Superconductivity can be achieved in various classes of Fe-based pnictides in different ways; for example, electron doping directly in the Fe-As layers [12,13] or by isovalent substitution of Fe with other elements such as Ru [14]. The superconductivity can also be achieved indirectly by electron or hole doping at other sites [1]; for example, by replacing O in $RFeAsO_{1-x}F_x$ by fluorine which is equivalent to electron doping in the system or by isovalent substitution of arsenic with phosphorus [15,16].

$EuTn_2As_2$ (Tn = transition metal, Cu, Ni, Cr, or Co) is an interesting member of the 122 family since the A site is occupied by the Eu^{2+}, which is an S-state rare-earth ion possessing a $4f^7$ electronic configuration with the electron spin $S = 7/2$ [17–21]. Among the Eu-based 122 compounds, $EuFe_2As_2$ is the most widely studied member. $EuFe_2As_2$ exhibits a spin-density-wave (SDW) transition in the Fe sublattice concomitant with a structural phase transition at 190 K. In addition, Eu^{2+} moments order in an A-type antiferromagnetic (AFM) structure at 19 K (ferromagnetic layers with moments along the **a** direction and the layers are antiferromagnetically aligned along the **c** direction) [22–24]. Superconductivity can be achieved in this system by substituting Eu with K or Na [9,25], as with P [26], and upon application of external pressure [27–29]. Doping as well as external pressure lead to a decrease of both the structural and Fe magnetic phase-transition temperatures and eventually superconductivity appears when both transitions are essentially suppressed [9].

However, an exception occurs in the presence of hole doping in the 122 family when Fe is replaced by either Cr [30] or Mn [31]. Doping of Cr and Mn causes suppression of the SDW and structural transitions but does not result in superconductivity. The absence of superconductivity in these systems remains an unresolved issue. A combined study of the physical properties and electronic-structure calculations in a closely related compound $BaCr_2As_2$ [32] conjectured that it is a metal with itinerant antiferromagnetism, similar to the parent phases of Fe-based superconductors but with slightly different magnetic structure. Neutron diffraction measurements on $BaFe_{2-x}Cr_xAs_2$ crystals reveal that the Cr doping in $BaFe_2As_2$ leads to suppression of the Fe SDW transition but the superconductivity (as usually observed in the case of other transition-metal doping) is prevented by a new competing magnetic order of G-type antiferromagnetism which becomes the dominant magnetic ground state for $x > 0.3$ [33]. Magnetic structure as well as ordering temperature of the Cr^{2+} moments is still unknown for the $BaCr_2As_2$. Similar to the $BaFe_{2-x}Cr_xAs_2$ systems, $BaFe_{2-x}Mn_xAs_2$ show gradual suppression of the SDW and structural transition as a function of Mn doping [34,35]. G-type magnetic structure is stabilized for the Mn^{2+} moments in $BaMn_2As_2$ [36].

Recently, single crystals of $EuCr_2As_2$ which crystallizes in the $ThCr_2Si_2$-type tetragonal structure with space group $I4/mmm$ were synthesized [37]. From Fig. 5, it can be seen that the Eu^{2+} ions reside on a body-centered tetragonal sublattice whereas Cr^{2+} ions reside on a primitive tetragonal sublattice. Magnetic structure of the Eu^{2+} moments as well as the Cr^{2+} moments in $EuCr_2As_2$ is unknown to date. It has been proposed based on electronic-structure calculations that the Cr^{2+} moments order most likely in a G-type antiferromagnetic structure at temperatures above 300 K whereas Eu^{2+} moments can either be ferromagnetic or antiferromagnetic below 21 K [37]. Determination of the magnetic structure is the first step towards understanding basic magnetic and electronic properties in this system, and the absence of superconductivity

*snandi@iitk.ac.in
†y.xiao@fz-juelich.de

in $EuCr_2As_2$. Here we report on the neutron diffraction studies of the nonsuperconducting $EuCr_2As_2$ single crystal to explore the details of the magnetic structure of the Eu^{2+} as well as of the Cr^{2+} moments. Our neutron diffraction experiments show that the Eu^{2+} moments order ferromagnetically along the **c** direction with an ordered moment of $6.2(5)\mu_B$ below $T_C = 21.0(1)$ K. The Cr^{2+} moments order below 680(40) K with moments also aligned along the **c** direction according to the G-type antiferromagnetic structure. The ordering temperature of the Cr^{2+} moments was determined from the magnetization measurement. No structural phase transition could be detected in the temperature range between 2 and 420 K.

II. EXPERIMENTAL DETAILS

Single crystals of $EuCr_2As_2$ were grown by using CrAs flux as described in Ref. [37]. For the diffraction measurements, a 43 mg as-grown single crystal of approximate dimensions 6 mm × 2.7 mm × 0.3 mm was selected. X-ray and neutron Laue measurements confirmed good quality of the sample and the tetragonal **c** axis is perpendicular to the flat plate-shaped crystal surface. The neutron diffraction experiment was performed on the four-circle diffractometer D10 at the Institut Laue–Langevin in Grenoble, France, by using a wavelength of 2.36 Å and a two-dimensional area detector mounted on the scattering arm for data collection. A pyrolytic graphite filter was employed to reduce the higher harmonic content to 10^{-4} of the primary beam energy. The sample was mounted on the cold finger of a He flow cryostat for a temperature variation between 2 and 420 K. For measurements of a few reflections, a vertically focusing pyrolytic graphite analyzer was used to reduce the background.

III. EXPERIMENTAL RESULTS

A. Macroscopic characterizations

Figure 1(a) shows temperature dependence of the magnetic susceptibility (M/H) for magnetic fields parallel to the a-b plane and the **c** direction measured by using a Quantum Design vibrating sample magnetometer (VSM). Below 300 K, magnetization was measured for magnetic fields parallel to the a-b plane at magnetic fields of 0.1, 3.0, and 5.0 T, respectively. Above 300 K, magnetization was measured for both the a-b plane and **c** direction by using the same magnetic fields for both temperature-increasing and -decreasing cycles. It can be easily seen that zero-field cooled magnetization rapidly increases below 100 K. From the derivative of the magnetic susceptibility measured with 0.1 T magnetic field (not shown), the ordering temperature of the Eu^{2+} moments, $T_C = 21.0(3)$ K, can be determined, which is also consistent with the neutron diffraction experiment presented in the next section. Above 300 K, magnetization for both directions looks identical and similar to a paramagnetic system. However, a close inspection of the inverse susceptibility and the difference between magnetic susceptibilities for both directions, as shown in the inset to Fig. 1(a), indicates an anomaly near 700 K. The high-temperature inverse magnetic susceptibility for magnetic field parallel to the **c** direction was fit with the modified Curie–Weiss law, $\chi = \chi_0 + C/(T + \theta)$, where χ_0 is the temperature-independent susceptibility, C is the Curie con-

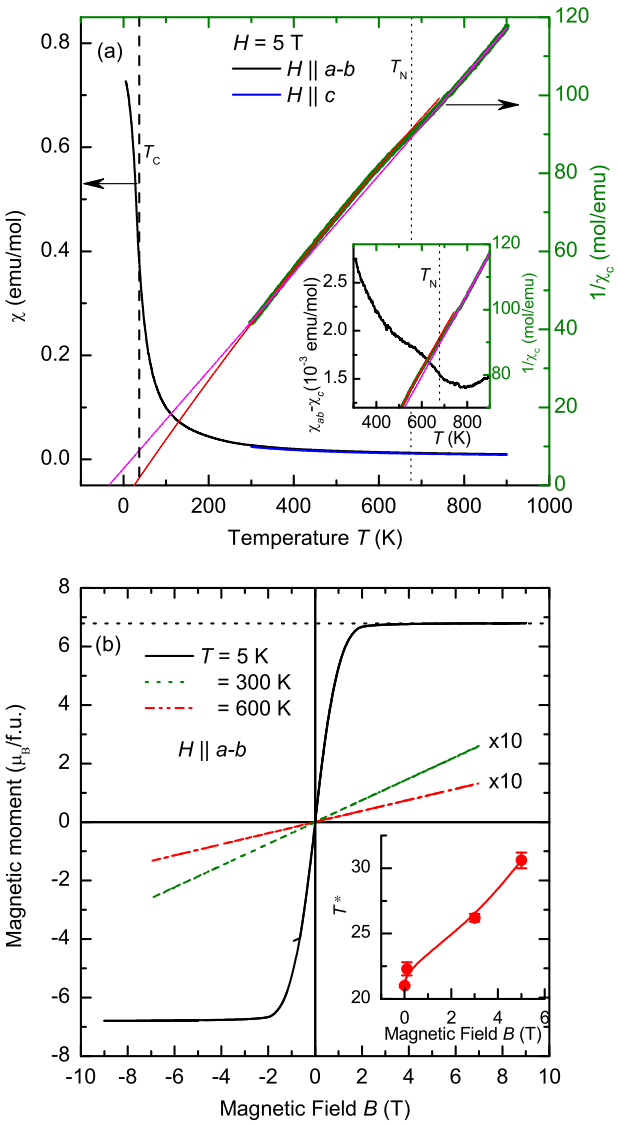

FIG. 1. (a) Temperature dependence of the magnetic susceptibility measured on heating of the zero-field cooled (ZFC) sample at an applied magnetic field of 5 tesla along the a-b plane and **c** direction, respectively, and inverse magnetic susceptibility for magnetic fields parallel to the **c** direction. For the magnetic field along the **c** direction, measurements were performed between 300 and 900 K. Inset shows difference of the magnetic susceptibilities between the a-b plane and the **c** direction and inverse magnetic susceptibility close to the phase transition. T_C and T_N denote ferromagnetic and antiferromagnetic transition temperatures of the Eu^{2+} and Cr^{2+} moments, respectively. The transition temperatures were determined from the minima of the derivative curve of the the magnetic susceptibility (for the Eu^{2+}) and from the change in slope of $1/\chi_c$ for the Cr^{2+}. Solid lines indicate Curie–Weiss fits to different temperature regions as described in the text. (b) M-H curves at $T = 5$, 300 and 600 K, respectively, for magnetic fields parallel to the a-b plane. For $T = 300$ and 600 K, magnetic susceptibility has been multiplied by a factor of 10 for better visibility. Dash-dotted horizontal line shows the saturation magnetic moment of the Eu^{2+}. Inset shows variation of the cross-over temperature (T^*) of the Eu^{2+} moments as a function of magnetic field, determined from the χ_{ab} measurements at various magnetic fields and neutron diffraction measurement (zero field).

stant, and θ is the Weiss temperature. For fitting below (from 300 to 600 K) and above (from 730 to 900 K) the observed anomaly as shown in Fig. 1 yields effective magnetic moments $\mu_{\text{eff}} = 7.07(3)\mu_B$, $7.96(2)\mu_B$ and $\theta = -25(1)$, 34(3) K, respectively. The deviation of inverse susceptibility from the Curie–Weiss behavior at 680(40) K indicates ordering of the Cr^{2+} moments at this temperature [38]. The obtained value of effective paramagnetic moment below the ordering of the Cr^{2+} moments is smaller than the theoretically expected value of $7.94\mu_B$ for a $S = \frac{7}{2}$ state of Eu^{2+} assuming a Landé g-factor of two. The increase of the effective paramagnetic moment above the ordering of the Cr^{2+} moments is most likely due to the contribution of Cr^{2+}. Moreover, the high ordering temperature of the Cr^{2+} moments is also expected from the electronic structure calculations [37]. Figure 1(b) shows isothermal magnetization as a function of magnetic field for fields parallel to the a-b plane at $T = 5$, 300, and 600 K, respectively. No hysteresis was observed between the field increasing and decreasing cycles. At $T = 5$ K, magnetization rapidly increases as the magnetic field increases up to 2 T and saturates above it. The saturation magnetic moment of $6.8(1)\mu_B$ is close to the theoretically expected value of $7\mu_B$. Magnetization parallel to the **c** direction shows similar behavior; however, the saturation magnetic field is smaller (0.5 T) as published in Ref. [37]. From the M-H measurements, it is not clear whether Eu^{2+} orders antiferromagnetically or ferromagnetically because of the linear slope of magnetization in small magnetic fields and the absence of hysteresis. Saturation of magnetic moment at a finite field as well as the linear slope is generally observed for a phase transition from an antiferromagnetic state to a field-induced ferromagnetic state. However, the magnetization increases rapidly below $T_C = 21.0$ K, at small applied magnetic field (0.05 T), as published in Ref. [37], indicates ferromagnetic ordering of the Eu^{2+} moments. At 300 and 600 K, the magnetization increases linearly with magnetic field, indicating paramagnetic or antiferromagnetic behavior of the system. The inset to the Fig. 1(b) shows variation of the cross-over temperature T^* of the Eu^{2+} magnetic order as a function of magnetic field determined from the minima of the derivative of the temperature dependent magnetization data at various magnetic fields. The cross-over temperature T^* indicates a cross over from the paramagnetic state to the ferromagnetic state without going through a phase transition since a paramagnetic to ferromagnetic phase transition does not occur in a finite magnetic field with applied field parallel to the easy axis [39]. The cross-over temperature increases with increasing magnetic field, reminiscent of that observed in other Eu based "122" systems [24,40].[1]

B. Neutron diffraction

For the parent compound $EuFe_2As_2$, it is well established that the Eu^{2+} moments order antiferromagnetically below $T_N = 19$ K whereas Fe moments undergo SDW transition below 190 K [22,23]. In this compound, Eu^{2+} moments adopt an A-type antiferromagnetic structure characterized by the propagation vector $\boldsymbol{\tau} = (0\ 0\ 1)$. Concomitant with the Fe magnetic order there is a structural phase transition from the tetragonal to orthorhombic crystal structure. Macroscopic measurements show clear signatures of these two transitions in $EuFe_2As_2$. However, for the case of $EuCr_2As_2$, only one phase transition can be clearly identified, i.e., the ordering of the Eu^{2+} moments at $T_C = 21$ K. Paramanik *et al.* [37] conjectured that the Eu^{2+} magnetic order can be either A-type antiferromagnetic or ferromagnetic or can even be a canted structure based on magnetization measurements.

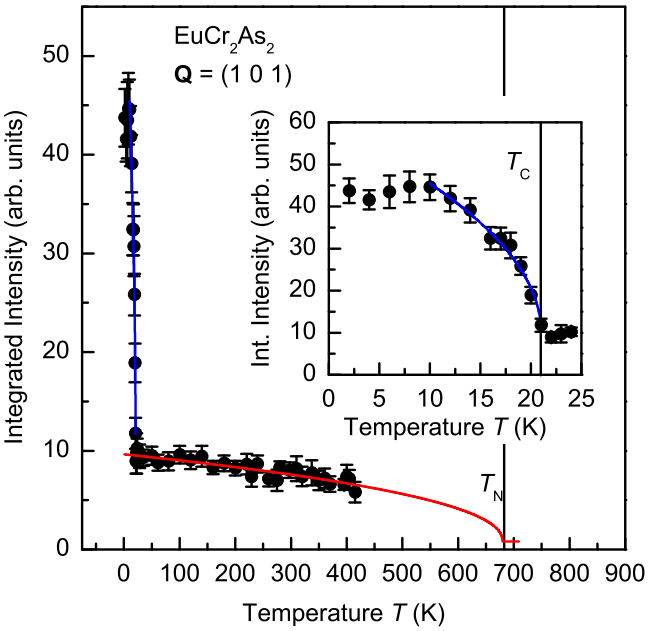

FIG. 2. Temperature dependence of the integrated intensity for the (1 0 1) reflection measured during heating of the sample. The inset shows details of the temperature dependence for the Eu^{2+} magnetic order. The solid lines are fits to the data as described in the text. The intensity of the (1 0 1) reflection above 21 K was normalized by that of the (2 2 0) reflection.

As a first step to solve the magnetic structure, precise knowledge of the nuclear structure is needed. Therefore, we measured the nuclear reflections allowed by the space group symmetry $I4/mmm$ at 30 K. Nuclear reflections after suitable absorption correction by using DATAP [41] can be reasonably well fit with the existing structure model except for a few reflections at low-**Q** region. The difference between the calculated and observed intensity [$I_{\text{calc.}} = 1.81$ vs $I_{\text{obs.}} = 20.5(2.0)$] is the largest for the (1 0 1) reflection. According to the nuclear structure established by x-ray diffraction, we expect close to zero intensity for this reflection. Extra intensity on top of the weak nuclear peak indicates the presence of magnetic contribution to this reflection and the magnetic propagation vector $\boldsymbol{\tau} = (0\ 0\ 0)$. Figure 2 shows the temperature dependence of this reflection measured upon heating the sample from 2 to 420 K. The intensity of the (1 0 1) reflection increases rapidly below 21 K, indicating Eu^{2+} magnetic order at this temperature with the same magnetic propagation vector $\boldsymbol{\tau} = (0\ 0\ 0)$. The integrated intensity ($I \sim m^2$, where m is the

[1]It should be noted that the PM to FM phase lines in Ref. [24,40] should be replaced by a dotted a line since a phase transition does not occur in a finite magnetic field with field parallel to the easy axis.

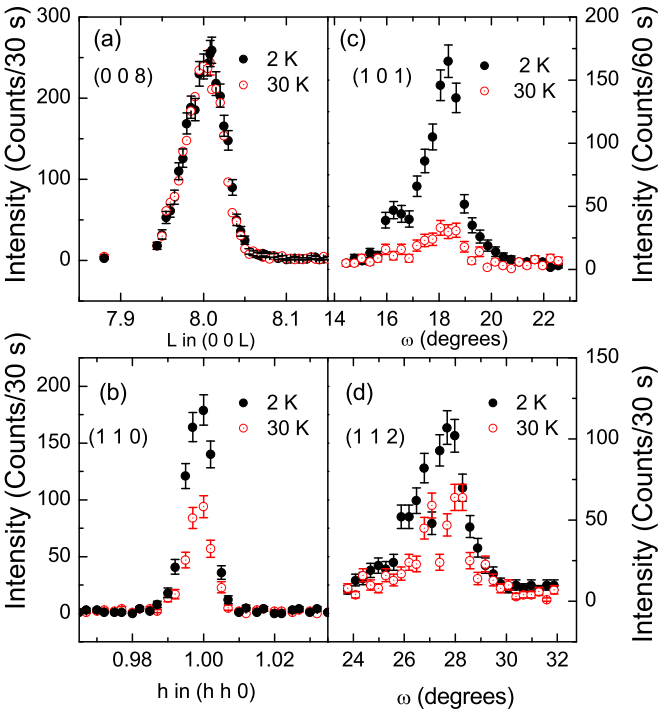

FIG. 3. (a), (b) L and h scans for the (0 0 8), (1 1 0) reflections, (c), (d) rocking scans for the (1 0 1) and (1 1 2) reflections at 2 and 30 K, respectively. Note that the magnetic intensity appears on top of the nuclear peaks and there is no change in the intensity for the (0 0 8) nuclear reflection.

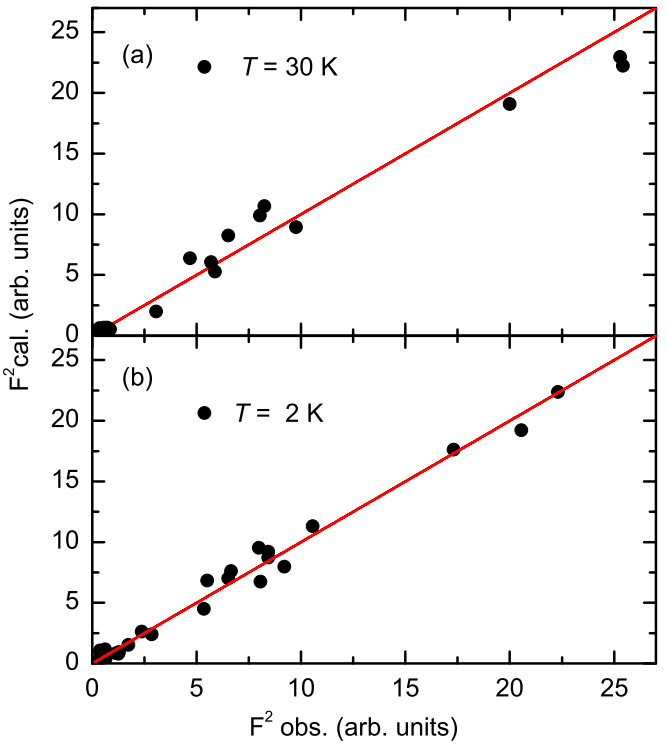

FIG. 4. (a), (b) Integrated intensities of the nuclear Bragg reflections collected at 30 and 2 K plotted against the calculated values. Magnetic intensity is superimposed with the nuclear reflections. See text for details of the crystal- and magnetic-structure models.

sublattice magnetization) can be fit with a power law of the form $I \sim (1 - \frac{T}{T_C})^{2\beta}$ to obtain the transition temperature of the Eu^{2+} magnetic order $T_C = 21.0(1)$ K and an exponent $\beta = 0.26(4)$. Above 21 K, the intensity of the (1 0 1) reflection decreases very slowly and is quite strong at 420 K, which is the highest temperature possible in the present experimental setup. The integrated intensity above 21 K was fit with the same power law with $T_N = 680$ K as found in Fig. 1, and with an exponent $\beta = 0.23(2)$ [42].

A scan along the [0 0 L] direction confirms the absence of the (0 0 l) reflections with l = odd that might arise from the A-type antiferromagnetic structure similar to the $EuFe_2As_2$ (not shown). Full width at half maximum (FWHM) of the (2 2 0) reflection shows no discernible variation over the temperature range 2–420 K, indicating the absence of the structural distortion. Rocking scans for several representative nuclear reflections at $T = 2$ and 30 K were performed to verify if there is any magnetic contribution superimposed on other weak or strong nuclear peaks. These scans are shown in Figs. 3(a)–3(d). It is clear from the L scans of the (0 0 8) reflection in Fig. 3(a) that they have identical intensities at 2 and 30 K, indicating the absence of magnetic signal at this position. However, the weakest nuclear reflections, (1 1 0) and (1 0 1), in Figs. 3(b) and 3(c), show a large variation in intensity between 2 and 30 K, indicating the presence of magnetic signal. For the strong nuclear reflection (1 1 2), the magnetic signal can also be observed on top of the nuclear signal, as shown in Fig. 3(d). These observations are very similar to the other Eu-based ferromagnetic 122 compounds [43–45] except for the presence of the strong intensity for the (1 0 1) and (1 1 0) reflections at 30 K due to the Cr^{2+} magnetic order. The absence of magnetic intensity for the (0 0 L) reflections with L even as well as strong intensity at the (1 1 0) reflection indicates that the Eu^{2+} moments are primarily aligned along the **c** direction.

C. Magnetic structure of Eu^{2+} and Cr^{2+} moments

We now turn to the determination of the magnetic moment configuration for the Cr^{2+} moments at 30 K. According to the representation analysis [46], both ferromagnetic and antiferromagnetic structures are possible for the Cr^{2+} moments with propagation vector $\boldsymbol{\tau} = (0\ 0\ 0)$. There are four magnetic representations possible for the Cr^{2+} moments, which we label as Γ_3, Γ_6, Γ_9, and Γ_{10}, respectively. The labeling of the propagation vector and the representation follows the scheme used by Kovalev [47]. Γ_3 and Γ_9 allow ferromagnetic alignment of the moments in the **c** direction and in the a-b plane, respectively, whereas Γ_6 and Γ_{10} allow antiferromagnetic alignment of the moments according to the G-type antiferromagnetic structure with moments along the **c** direction and in the a-b plane, respectively. Linear slope in magnetization at 300 and 600 K indicates antiferromagnetic structure of the Cr^{2+} moments. The integrated intensities of total 101 nuclear reflections (out of which 25 are independent) were collected at 30 K and were analyzed by using FULLPROF [48] after necessary absorption correction using DATAP [41]. Figure 4(a) shows fitting of the reflections according to the G-type antiferromagnetic structure with moments along

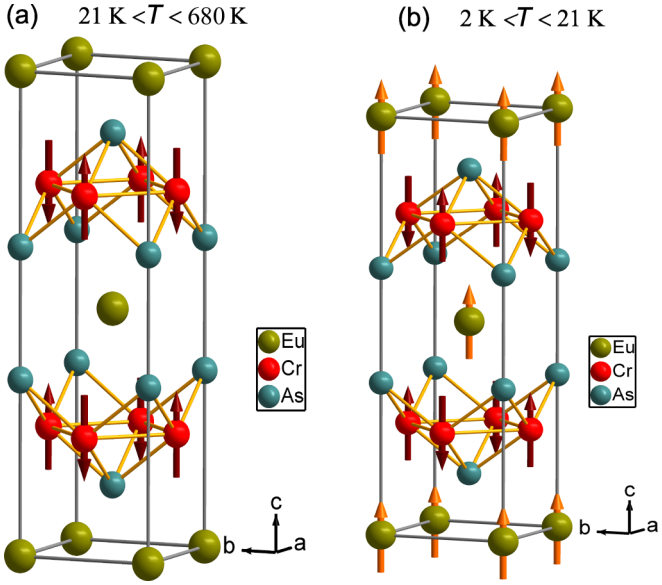

FIG. 5. The ground-state magnetic structure of $EuCr_2As_2$ for (a) 21 K $\leqslant T \leqslant$ 680 K, and (b) 2 K $\leqslant T \leqslant$ 21 K as determined by single-crystal neutron diffraction measurements.

the **c** direction *i.e.* Γ_6 magnetic representation. The fitting parameters and goodness of fit values are shown in Table I. For the two *G*-type antiferromagnetic structures, moments within the *a*-*b* plane (Γ_{10}) highly underestimate the magnetic intensity for the (1 0 1) reflection and thus can be discarded. The ferromagnetic structures, Γ_3 and Γ_9, produce much larger goodness-of-fit values (χ^2 and *R* factors) and thus can also be rejected. Combining the fact that the magnetic susceptibility is lower for the **c** direction than in the *a*-*b* plane (see inset to Fig. 1), it is most likely that the Cr^{2+} moments order along the **c** direction according to the *G*-type antiferromagnetic structure shown in Fig. 5(a).

Below 21 K, both the Eu^{2+} and the Cr^{2+} moments are ordered. Here we note that only ferromagnetic structures with magnetic moments along the three crystallographic directions **a**, **b**, **c** are allowed by symmetry for the Eu^{2+} moments and the same set of magnetic representations are possible for the Cr^{2+} moments. No antiferromagnetic structure with propagation vector $\boldsymbol{\tau} = (0\ 0\ 0)$ is possible in this case for symmetry reasons for the Eu^{2+} moments. Since for magnetic neutron scattering, the scattered intensity is sensitive to the component of the magnetic moment perpendicular to **Q**, absence of magnetic intensity for the nuclear (0 0 *L*) reflections [see Fig. 3(a)] indicates that the moments are primarily aligned along the **c** direction. The integrated intensities of the total 111 reflections (out of which 28 are independent) were collected at 2 K and fit with the *G*-type antiferromagnetic structure (Γ_6) of Cr^{2+} along with the different ferromagnetic structures possible for the Eu^{2+} moments by using FULLPROF [48] at 2 K. As expected, the best fit was obtained for the ferromagnetic structure of the Eu^{2+} moments aligned along the **c** direction (Γ_3 magnetic representation for the Eu^{2+}) and with the *G*-type antiferromagnetic structure of the Cr^{2+} moments (Γ_6 magnetic representation). The observed intensity is plotted against the calculated integrated intensity in Fig. 4(b). The magnetic structure and associated fitting parameters at 2 K are shown in Fig. 5(b) and Table I, respectively. The ordered moments for Eu^{2+} and Cr^{2+} amount to $6.2(5)\mu_B$ and $1.7(4)\mu_B$, respectively, at 2 K. While the ordered moment of the Eu^{2+} is close to the theoretically expected value of $7.0\mu_B$, the ordered moment of the Cr^{2+} (d^4) is quite low compared to the theoretically expected high-spin moment of Cr^{2+} of $4.0\mu_B$ but large compared to the low-spin moment of $0.0\mu_B$ assuming a *g* factor of two. The reduced moment of Cr^{2+} is most likely due to the itinerant nature of the Cr magnetism in $EuCr_2As_2$ [49]. Assuming a spin value corresponding to the ordered magnetic moments of both the sublattices, we expect $\mu_{\text{eff}} = 7.0(1.0)$, $8.8(1.5)\mu_B$ for the temperatures below and above the ordering of Cr^{2+}, respectively, which is broadly in agreement with magnetization measurement presented in Sec. III A.

TABLE I. Refined results of the crystal and magnetic structures for $EuCr_2As_2$ at 30 and 2 K using space group $I4/mmm$ (space group No. 139). Thermal parameters were fixed according to the previous measurement on $EuFe_2As_2$ [23].

	Position in $I4/mmm$				
Atom	Site	*x*	*y*	*z*	B (Å^2)
Eu	2*a*	0	0	0	0.8
Cr	4*d*	$\frac{1}{2}$	0	$\frac{1}{4}$	0.3
As	4*e*	0	0	0.368(3)	0.3
$a = 3.863(2)$ Å, $c = 12.867(4)$ Å					
$T = 30$ K, Extinction g (rad^{-1}) $= 1.0(5)$, $\mu_{Cr} = 1.7(4)\mu_B$,					
R_{F^2}, R_F, χ^2: 14.5, 12.2, 2.5					
$T = 2$ K, g (rad^{-1}) $= 1.0(5)$, $\mu_{Cr} = 1.7(4)\mu_B$, $\mu_{Eu} = 6.2(5)\mu_B$					
R_{F^2}, R_F, χ^2: 10.5, 8.3, 2.8					

IV. CONCLUSION

In conclusion, the magnetic structure of the Eu^{2+} and Cr^{2+} moments in the nonsuperconducting parent compound $EuCr_2As_2$ has been determined by using neutron diffraction measurements. While the Eu^{2+} moments order ferromagnetically with moments aligned along the **c** direction below $T_C = 21.0(1)$ K, the ordering temperature of the Cr^{2+} moments is found to be at the very high temperature of 680(40) K. The Cr^{2+} moments order in a *G*-type antiferromagnetic structure with moments also aligned along the **c** direction. The higher ordering temperature of the Cr^{2+} moments indicates that the exchange interactions among the Cr^{2+} moments are very strong and that the Eu and Cr sublattices are completely decoupled.

ACKNOWLEDGMENTS

S.N. would like to acknowledge S. Mayr for her assistance with the orientation of the crystals and Philippe Decarpentrie for his technical assistance with the cryostat throughout the experiment. S.N. would further like to thank V. Subrahmanyam, A. K. Gupta, and Amit Dutta for fruitful discussion on phase transition and critical phenomena.

[1] Y. Kamihara, T. Watanabe, M. Hirano, and H. Hosono, J. Am. Chem. Soc. **130**, 3296 (2008).

[2] D. C. Johnston, Adv. Phys. **59**, 803 (2010).

[3] H. Takahashi, K. Igawa, K. Arii, Y. Kamihara, M. Hirano, and H. Hosono, Nature (London) **453**, 376 (2008).

[4] X. H. Chen, T. Wu, G. Wu, R. H. Liu, H. Chen, and D. F. Fang, Nature (London) **453**, 761 (2008).

[5] Z.-A. Ren, W. Lu, J. Yang, W. Yi, X.-L. Shen, Z.-C. Li, G.-C. Che, X.-L. Dong, L.-L. Sun, F. Zhou, and Z.-X. Zhao, Chin. Phys. Lett. **25**, 2215 (2008).

[6] F.-C. Hsu, J.-Y. Luo, K.-W. Yeh, T.-K. Chen, T.-W. Huang, P. M. Wu, Y.-C. Lee, Y.-L. Huang, Y.-Y. Chu, D.-C. Yan, and M.-K. Wu, Proc. Natl. Acad. Sci. USA **105**, 14262 (2008).

[7] J. Guo, S. Jin, G. Wang, S. Wang, K. Zhu, T. Zhou, M. He, and X. Chen, Phys. Rev. B **82**, 180520 (2010).

[8] M. Rotter, M. Tegel, and D. Johrendt, Phys. Rev. Lett. **101**, 107006 (2008).

[9] H. S. Jeevan, Z. Hossain, D. Kasinathan, H. Rosner, C. Geibel, and P. Gegenwart, Phys. Rev. B **78**, 092406 (2008).

[10] K. Sasmal, B. Lv, B. Lorenz, A. M. Guloy, F. Chen, Y.-Y. Xue, and C.-W. Chu, Phys. Rev. Lett. **101**, 107007 (2008).

[11] Z. Bukowski, S. Weyeneth, R. Puzniak, J. Karpinski, and B. Batlogg, Physica C (Amsterdam, Neth.) **470**, S328 (2010).

[12] A. Leithe-Jasper, W. Schnelle, C. Geibel, and H. Rosner, Phys. Rev. Lett. **101**, 207004 (2008).

[13] D. Kasinathan, A. Ormeci, K. Koch, U. Burkhardt, W. Schnelle, A. Leithe-Jasper, and H. Rosner, New J. Phys. **11**, 025023 (2009).

[14] W. Schnelle, A. Leithe-Jasper, R. Gumeniuk, U. Burkhardt, D. Kasinathan, and H. Rosner, Phys. Rev. B **79**, 214516 (2009).

[15] C. Wang, S. Jiang, Q. Tao, Z. Ren, Y. Li, L. Li, C. Feng, J. Dai, G. Cao, and Z. A. Xu, Europhys. Lett. **86**, 47002 (2009).

[16] S. Jiang, H. Xing, G. Xuan, C. Wang, Z. Ren, C. Feng, J. Dai, Z. Xu, and G. Cao, J. Phys.: Condens. Matter **21**, 382203 (2009).

[17] R. Marchand and W. Jeitschko, J. Solid State Chem. **24**, 351 (1978).

[18] R. Nagarajan, G. K. Shenoy, L. C. Gupta, and E. V. Sampathkumaran, Phys. Rev. B **32**, 2846 (1985).

[19] M. Bishop, W. Uhoya, G. Tsoi, Y. K. Vohra, A. S. Sefat, and B. C. Sales, J. Phys.: Condens. Matter **22**, 425701 (2010).

[20] K. Sengupta, P. L. Paulose, E. V. Sampathkumaran, T. Doert, and J. P. F. Jemetio, Phys. Rev. B **72**, 184424 (2005).

[21] V. K. Anand and D. C. Johnston, Phys. Rev. B **91**, 184403 (2015).

[22] J. Herrero-Martín, V. Scagnoli, C. Mazzoli, Y. Su, R. Mittal, Y. Xiao, T. Brueckel, N. Kumar, S. K. Dhar, A. Thamizhavel, and L. Paolasini, Phys. Rev. B **80**, 134411 (2009).

[23] Y. Xiao, Y. Su, M. Meven, R. Mittal, C. M. N. Kumar, T. Chatterji, S. Price, J. Persson, N. Kumar, S. K. Dhar, A. Thamizhavel, and Th. Brueckel, Phys. Rev. B **80**, 174424 (2009).

[24] Y. Xiao, Y. Su, W. Schmidt, K. Schmalzl, C. M. N. Kumar, S. Price, T. Chatterji, R. Mittal, L. J. Chang, S. Nandi, N. Kumar, S. K. Dhar, A. Thamizhavel, and Th. Brueckel, Phys. Rev. B **81**, 220406 (2010).

[25] Y. Qi, Z. Gao, L. Wang, D. Wang, X. Zhang, and Y. Ma, New J. Phys. **10**, 123003 (2008).

[26] Z. Ren, Q. Tao, S. Jiang, C. Feng, C. Wang, J. Dai, G. Cao, and Z. Xu, Phys. Rev. Lett. **102**, 137002 (2009).

[27] C. F. Miclea, M. Nicklas, H. S. Jeevan, D. Kasinathan, Z. Hossain, H. Rosner, P. Gegenwart, C. Geibel, and F. Steglich, Phys. Rev. B **79**, 212509 (2009).

[28] T. Terashima, M. Kimata, H. Satsukawa, A. Harada, K. Hazama, S. Uji, H. S. Suzuki, T. Matsumoto, and K. Murata, J. Phys. Soc. Jpn. **78**, 083701 (2009).

[29] Y. Tokiwa, S.-H. Hübner, O. Beck, H. S. Jeevan, and P. Gegenwart, Phys. Rev. B **86**, 220505 (2012).

[30] A. S. Sefat, D. J. Singh, L. H. VanBebber, Y. Mozharivskyj, M. A. McGuire, R. Jin, B. C. Sales, V. Keppens, and D. Mandrus, Phys. Rev. B **79**, 224524 (2009).

[31] Y. Liu, D. Sun, J. Park, and C. Lin, Physica C (Amsterdam, Neth.) **470**, S513 (2010).

[32] D. J. Singh, A. S. Sefat, M. A. McGuire, B. C. Sales, D. Mandrus, L. H. VanBebber, and V. Keppens, Phys. Rev. B **79**, 094429 (2009).

[33] K. Marty, A. D. Christianson, C. H. Wang, M. Matsuda, H. Cao, L. H. VanBebber, J. L. Zarestky, D. J. Singh, A. S. Sefat, and M. D. Lumsden, Phys. Rev. B **83**, 060509 (2011).

[34] M. G. Kim, A. Kreyssig, A. Thaler, D. K. Pratt, W. Tian, J. L. Zarestky, M. A. Green, S. L. Bud'ko, P. C. Canfield, R. J. McQueeney, and A. I. Goldman, Phys. Rev. B **82**, 220503 (2010).

[35] D. S. Inosov, G. Friemel, J. T. Park, A. C. Walters, Y. Texier, Y. Laplace, J. Bobroff, V. Hinkov, D. L. Sun, Y. Liu, R. Khasanov, K. Sedlak, Ph. Bourges, Y. Sidis, A. Ivanov, C. T. Lin, T. Keller, and B. Keimer, Phys. Rev. B **87**, 224425 (2013).

[36] Y. Singh, M. A. Green, Q. Huang, A. Kreyssig, R. J. McQueeney, D. C. Johnston, and A. I. Goldman, Phys. Rev. B **80**, 100403 (2009).

[37] U. B. Paramanik, R. Prasad, C. Geibel, and Z. Hossain, Phys. Rev. B **89**, 144423 (2014).

[38] A clear difference is observed between the observed and calculated curves when the Curie–Weiss fit deviates more than 0.2% from the observed one. Therefore, we have taken this as a criterion for determining upper and lower bounds of T_N and T_N itself.

[39] M. F. Collins, in *Magnetic Critical Scattering* (Oxford University Press, New York, 1989), p. 5.

[40] S. Nandi, W. T. Jin, Y. Xiao, Y. Su, S. Price, D. K. Shukla, J. Strempfer, H. S. Jeevan, P. Gegenwart, and T. Brückel, Phys. Rev. B **89**, 014512 (2014).

[41] P. Coppens, L. Leiserowitz, and D. Rabinovich, Acta Crystallogr. **18**, 1035 (1965).

[42] With a free fit, unreasonable values are obtained. Therefore, we fixed T_N. The exponent β does not carry any physical significance in the present case. To obtain a physically meaningful β, the temperature dependence must be fit very close to the ordering temperature.

[43] W. T. Jin, S. Nandi, Y. Xiao, Y. Su, O. Zaharko, Z. Guguchia, Z. Bukowski, S. Price, W. H. Jiao, G. H. Cao, and Th. Brückel, Phys. Rev. B **88**, 214516 (2013).

[44] W. T. Jin, W. Li, Y. Su, S. Nandi, Y. Xiao, W. H. Jiao, M. Meven, A. P. Sazonov, E. Feng, Y. Chen, C. S. Ting, G. H. Cao, and Th. Brückel, Phys. Rev. B **91**, 064506 (2015).

[45] S. Nandi, W. T. Jin, Y. Xiao, Y. Su, S. Price, W. Schmidt, K. Schmalzl, T. Chatterji, H. S. Jeevan, P. Gegenwart, and Th. Brückel, Phys. Rev. B **90**, 094407 (2014).

[46] A. S. Wills, Physica B (Amsterdam, Neth.) **276-278**, 680 (2000).

[47] O. V. Kovalev, in *Representations of the Crystallographic Space Groups* (Gordon and Breach Science Publishers, Amsterdam, 1993).

[48] J. Rodríguez-Carvajal, Physica B (Amsterdam, Neth.) **192**, 55 (1993).

[49] T. Yildirim, Physica C (Amsterdam, Neth.) **469**, 425 (2009).